Macro-velocity model building in a Laplace-domain waveform inversion

Changsoo Shin*, Seoul National University, Seoul, Republic of Korea
css@model.snu.ac.kr
and
Wansoo Ha, Seoul National University, Seoul, Republic of Korea

GeoConvention 2012:Vision

Summary

We explain why Laplace-domain inversion yields long-wavelength velocity models. Unlike an inversion in the time and frequency domains, Laplace-domain inversion results of real marine data are macro-velocity models, due to the smooth gradient direction in the Laplace domain. The gradient direction is calculated by multiplying the virtual source and the back-propagated wavefield. The virtual source has long-wavelength features following the wavefield and the velocity used in an inversion. The back-propagated wavefield shows mild variations except for the near surface area, in spite of the short-wavelength components in the residual. Since the high-wavenumber components of the Green's function are attenuated more rapidly than the low-wavenumber components. The Green's function can be thought as a low-wavenumber pass filter. Accordingly, the gradient direction and the inversion results are smooth. An inversion example of field data acquired in the Gulf of Mexico shows a long-wavelength gradient and confirms the macro-velocity generation feature of the Laplace-domain inversion technique.

Introduction

Full waveform inversion is a method to delineate the subsurface structures by minimizing the differences between the observed and modeled wavefield (Tarantola, 1984). Its algorithm is promising, however, local minima is a serious problem when inverting field data (Bunks et al., 1995). Inversions of reflection data in the time and frequency domains tend to invert short-wavelength features only (Jannane et al., 1989) and fall into a local minimum. An accurate starting velocity or low-frequency data is required in order to avoid the local-minima problem (Virieux and Operto, 2009).

Shin and Cha suggested a full waveform inversion in the Laplace domain as an alternative to inversions in the time and frequency domains (Shin and Cha, 2008). A Laplace-domain inversion can start from scratch and yield a large-scale velocity model from field data (Shin and Cha, 2008). A Laplace-domain inversion result can serve as a background velocity or a starting model for a subsequent inversion in the time or frequency domain (Shin and Ha, 2008).

Ha et al. (2010) and Pyun et al. (2011) partially explained why Laplace-domain inversion yields a smooth velocity model using synthetic examples. They found that the residuals in a Laplace-domain inversion are very smooth regardless of the damping constants for synthetic datasets. When compared to a frequency-domain inversion, the shapes of Laplace-domain residuals are similar to those of low-frequency residuals in a frequency-domain inversion. Gradient directions in a Laplace-domain inversion are smooth since the gradients are obtained by back-propagating these long-wavelength residuals. They can be compared to the gradients obtained using very low-frequency components in a frequency-domain inversion. However, residuals observed in a field data inversion in the Laplace domain contains short-wavelength features, due to noise in the observed data. They resemble high-frequency residuals

of a frequency-domain inversion rather than low-frequency residuals. Therefore, the explanation above is not valid in real-data cases.

In this study, we show why Laplace-domain inversion results are still smooth in real-data inversions. First, we review the Laplace-domain inversion and Cagniard deHoop's method to solve the scalar wave equation. Then we explain the long-wavelength feature of the Laplace-domain inversion using the Laplace-domain Green's function. We also present a field data example whose residuals contain short-wavelength components.

Laplace-domain inversion

We briefly review the inversion algorithm in the Laplace domain (Shin and Cha, 2008). The wave equation in the Laplace domain can be expressed using matrices as

$$s^2\mathbf{Mu} + \mathbf{Ku} = \mathbf{Su} = \mathbf{f}, \tag{1}$$

where s is a damping constant, $\mathbf{u}$ is a Laplace-domain wavefield vector, $\mathbf{M}$ is a mass matrix, $\mathbf{K}$ is a stiffness matrix, $\mathbf{S}$ is an impedance matrix, and $\mathbf{f}$ is a source vector (Marfurt, 1984). We used the logarithmic objective function (Shin and Min, 2006) for each damping constant as

$$E = \sum_{i=1}^{N_s}\sum_{j=1}^{N_r}\left(\ln\frac{\tilde{u}_{ij}}{\tilde{d}_{ij}}\right)^2, \tag{2}$$

where N_s is the number of shots, N_r is the number of receivers, $\tilde{u}$ is the modeled wavefield, and $\tilde{d}$ is the observed wavefield. The gradient direction of this objective function is

$$\frac{\partial E}{\partial p_k} = \sum_{i=1}^{N_s}\left(\mathbf{v}_k\right)^T\mathbf{S}^{-1}\mathbf{r}_i, \tag{3}$$

where p_k is the k-th model parameter, $\mathbf{v}_k$ is the virtual source vector and $\mathbf{r}_i$ is the residual vector defined as follow:

$$\mathbf{v}_k = \frac{\partial\mathbf{S}}{\partial p_k}\tilde{\mathbf{u}}_i, \tag{4}$$

$$\mathbf{r}_i = \left[\begin{array}{ccccccc} \frac{1}{\tilde{u}_{i1}}\ln\frac{\tilde{u}_{i1}}{\tilde{d}_{i1}} & \frac{1}{\tilde{u}_{i2}}\ln\frac{\tilde{u}_{i2}}{\tilde{d}_{i2}} & \cdots & \frac{1}{\tilde{u}_{iN_r}}\ln\frac{\tilde{u}_{iN_r}}{\tilde{d}_{iN_r}} & 0 & \cdots & 0 \end{array}\right]^T. \tag{5}$$

The velocity model is updated by the sum of each gradient direction normalized by the pseudo-Hessian (Shin and Cha, 2008) as

$$p_k^{l+1} = p_k^l - \alpha\sum_s\frac{\sum_{i=1}^{N_s}\left(\mathbf{v}_k\right)^T\mathbf{S}^{-1}\mathbf{r}_i}{\sum_{i=1}^{N_s}\left(\mathbf{v}_k\right)^T\mathbf{v}_k + \lambda}, \tag{6}$$

where l is the iteration number, α is a step length, and λ is a stabilizing constant (Shin and Cha, 2008).

Laplace-domain Green's functions

We review Cagniard deHoop's method (Aki and Richards, 2002) to solve the scalar wave equation in a homogeneous, unbounded medium. We can obtain the kernel of the solution in the k_x - z - s domain using this method. The 2-dimensional scalar wave equation can be expressed as

$$\frac{1}{c^2}\frac{\partial^2 u(x,z,t)}{\partial t^2} = A_0\delta(x)\delta(z)\delta(t) + \nabla^2 u(x,z,t), \tag{7}$$

where $u(x,z,t)$ is the wavefield and A_0 is the amplitude of an impulse source. If we take the Fourier transform of the equation with respect to x and the Laplace transform with respect to the time, we can obtain the following equation.

$$\left(\frac{s^2}{c^2} + k_x^2\right) u(k_x,z,s) = A_0\delta(z) + \frac{\partial^2 u(k_x,z,s)}{\partial z^2}. \tag{8}$$

The solution of the equation can be expressed as

$$u(k_x,z,s) = ae^{nz} + be^{-nz}, \tag{9}$$

where

$$n^2 = \frac{s^2}{c^2} + k_x^2. \tag{10}$$

By applying appropriate boundary and continuity conditions, we can obtain the analytic solution as follows (Aki and Richards, 2002).

$$u(k_x,z,s) = \frac{A_0}{2\sqrt{\frac{s^2}{c^2} + k_x^2}} e^{-\sqrt{\frac{s^2}{c^2}+k_x^2}|z|}. \tag{11}$$

We can further obtain the x-z-s domain solution by an inverse Fourier transform as

$$u(x,z,s) = \frac{A_0}{4\pi}\int_{-\infty}^{\infty} \frac{e^{-\sqrt{\frac{s^2}{c^2}+k_x^2}|z|} e^{ik_x x}}{\sqrt{\frac{s^2}{c^2} + k_x^2}} dk_x . \tag{12}$$

Since the exponential kernel dominate the behavior of the wavefield, we will focus on the kernel. The kernel of the 3-dimensional solution and those of the frequency-domain also can be obtained by a similar derivation (Officer, 1958; Schneider, 1978; Aki and Richards, 2002). They are shown in Table 1.

	Laplace domain	Frequency domain
2D	$\mathrm{e}^{-\sqrt{\frac{s^2}{c^2}+k_x^2}\lvert z\rvert}$	$\mathrm{e}^{-i\sqrt{\frac{\omega^2}{c^2}-k_x^2}\lvert z\rvert}$
3D	$\mathrm{e}^{-\sqrt{\frac{s^2}{c^2}+k_x^2+k_y^2}\lvert z\rvert}$	$\mathrm{e}^{-i\sqrt{\frac{\omega^2}{c^2}-k_x^2-k_y^2}\lvert z\rvert}$

Table 1: The kernels of the 2D and 3D scalar wave equations in the Laplace and Frequency domains.

The reason Laplace-domain wavefields are smooth can be explained using the kernels. As we can see from the kernels, Laplace-domain wavefields are damped out quickly as the wavenumber, depth, and the damping constant increase. The kernel acts as a low-wavenumber pass filter. Therefore, effect of high-wavenumber contents on the Laplace-domain wavefield is limited, and the wavefields in the Laplace domain shows long-wavelength features, except for the near-source area. The high-wavenumber components at the near-source area will be discussed later, in the numerical example section.

The gradient direction in a Laplace-domain inversion shows long-wavelength features (Ha et al., 2010) due to the smooth wavefields. The gradient direction can be calculated by multiplying the virtual source vector and the back-propagated wavefield (equation 3). The virtual source is a multiplication between the partial derivative of the impedance matrix and a smooth, modeled wavefield (equation 4). The partial derivative of the impedance matrix is expressed as

$$\frac{\partial \mathbf{S}}{\partial p_k} = s^2 \frac{\partial \mathbf{M}}{\partial p_k}. \tag{13}$$

The mass matrix in equation 13 depends on the velocity (Cohen, 2002). We generally start an inversion from a large-scale velocity model and therefore, the virtual source shows mild variations. The back-propagated wavefield also has long-wavelength features since it is a superposition of smooth impulse responses where each impulse corresponds to the residual at each receiver position. Accordingly, the gradient direction and inversion results show long-wavelength features in the Laplace domain.

On the other hand, frequency-domain wavefield oscillates due to the complex-valued exponent. Accordingly, the gradient direction in a frequency-domain inversion also oscillates. When the frequency is low, the oscillation is not large and the gradient direction is similar to that of the Laplace-domain. It shows long-wavelength features. However, the shape of the gradient at a high frequency is highly oscillatory and shows short-wavelength features (Ha et al., 2010; Pyun et al., 2011).

Numerical Examples

We demonstrate the property of long-wavelength velocity generation using a field dataset acquired in the Gulf of Mexico. The dataset contains 399 shots and each shot has 408 receivers. The intervals between shots are 50 m and those between receivers are 25 m. The maximum recording time is 12 s and the maximum offset is 10,292 m. Figure 1 shows a shot gather up to 6 s. We muted noise appearing before the first arrival for a correct Laplace transformation.

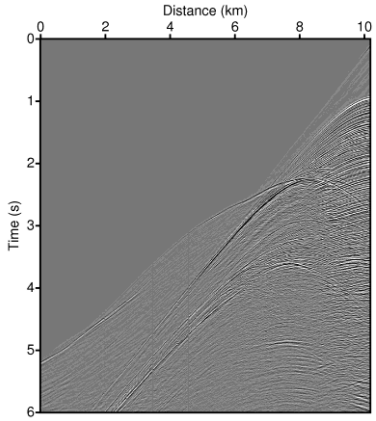

Figure 1. The 200th shot gather extracted from a dataset acquired in the Gulf of Mexico.

We transformed the shot gather to the Laplace domain for the damping constant of 2 and 12. The Laplace-domain wavefields show short-wavelength features (Figure 2). As we can expect from equation 11, the short-wavelength features diminish at the high damping constant. Figure 3 shows residuals defined in equation 5. The modeled wavefield was calculated from a two-layer velocity model. The upper layer in the velocity model was a constant-velocity water layer and the velocity of the lower layer was increased linearly with the depth. Since the residual at the damping constant of 2 contains high-wavenumber components, we present the back-propagated wavefield of this residual (Figure 4). The back-propagated wavefield is very smooth except for the surface where the receivers are located. Accordingly, the gradient direction, which is the multiplication between the virtual source and the back-propagated wavefield, is smooth except for the surface area. One of important advantages in a marine-data inversion over a land-data inversion is that we know the velocity of the water. Therefore, we don't use the gradient at the water layer. The normalized gradient of the 200th shot is a long-wavelength gradient as shown in Figure 5a. We inverted the data using 11 damping constants from 2 to 12. Figure 5b shows the large-scale inversion result obtained using the smooth gradients. It shows high-velocity salt structures clearly. A migration image of this dataset obtained using a Laplace-domain inversion result can be found in Shin and Cha (2008).

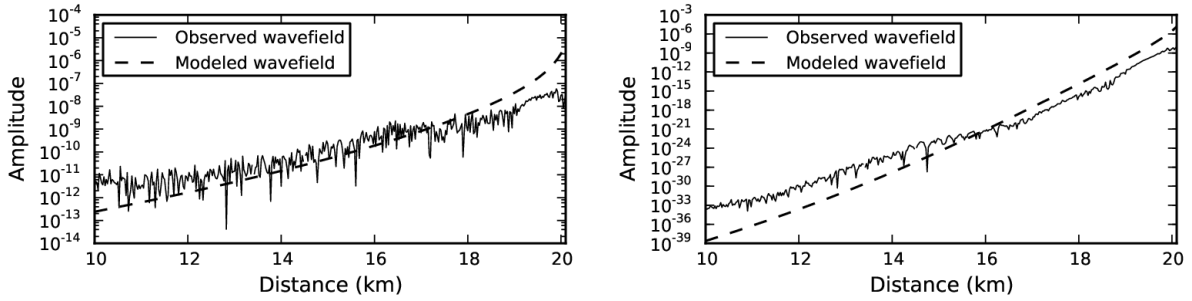

Figure 2. The observed and modeled wavefields in the Laplace domain with the damping constant of (a) 2 and (b) 12, corresponding to the 200th shot gather.

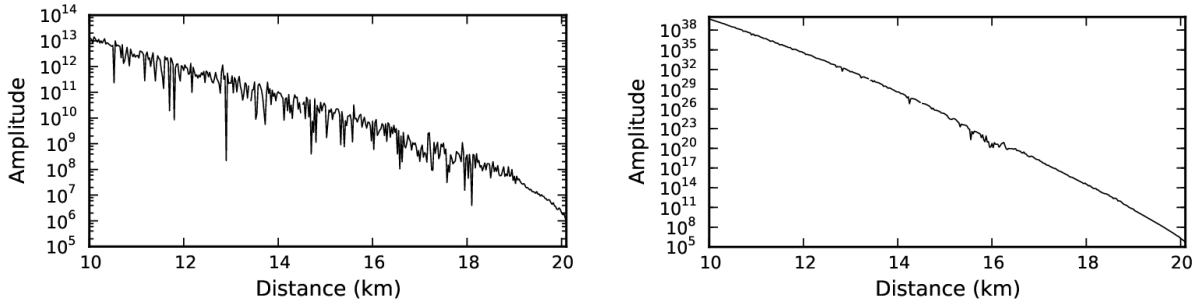

Figure 3. The residual (equation 5) with the damping constant of (a) 2 and (b) 12, corresponding to the 200th shot gather.

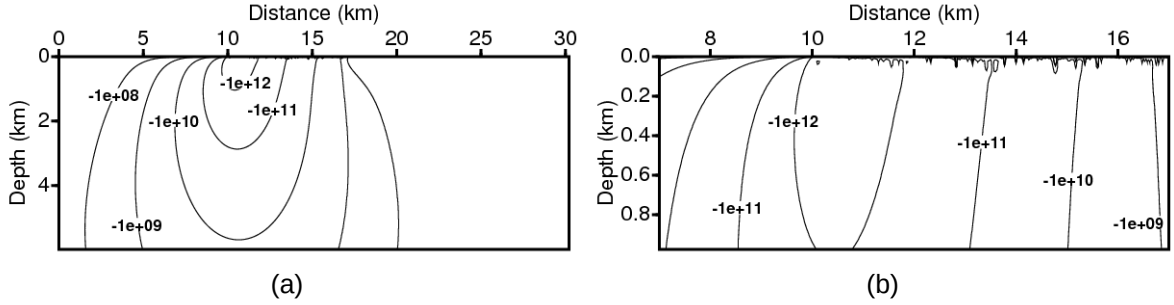

Figure 4. (a) The back-propagated wavefield ($\mathbf{s}^{-1}\mathbf{r}_{200}$ in equation 3) for the damping constant of 2, and (b) its magnified view.

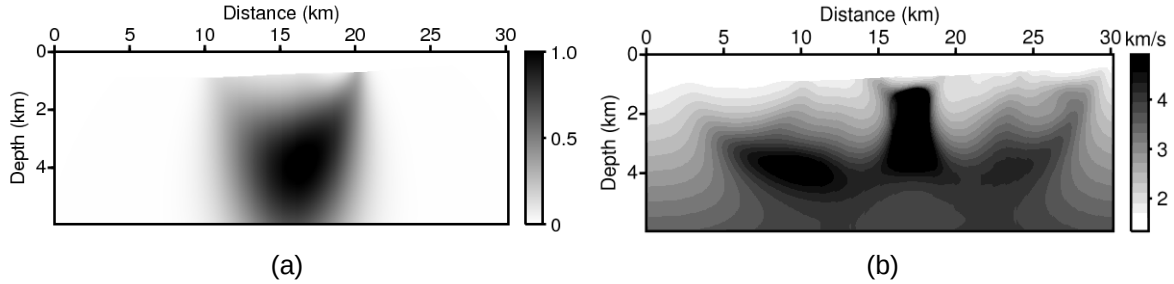

Figure 5. (a) The normalized gradient direction corresponding to the 200th shot, and (b) the inversion result.

The discussion above does not hold true for field data acquired on a land or ocean bottom since we cannot remove the gradient of a water layer. Therefore, land-data inversion in the Laplace domain can suffer from high-wavenumber gradients at the surface area. There is no published real land-data inversion example in the Laplace domain yet. One might need to apply a process to remove the short-wavelength features at the surface to invert real land-data in the Laplace domain.

Conclusions

We showed why Laplace-domain inversion results of marine data show mild variations. The gradient direction in the inversion is a multiplication between the virtual source and the back-propagated wavefield. The virtual source is calculated from the modeled wavefield and the mass matrix, which depends on the velocity model. It is smooth following the modeled wavefield and the velocity. The back-propagated wavefield is obtained by exciting the short-wavelength residual as a source at the receiver location. The back-propagated wavefield has long-wavelength features except for the surface area since the high-wavenumber parts of the Laplace-domain Green's function are damped out more rapidly than the low-wavenumber parts. In a marine data inversion, we ignore the gradient at the water layer and the short-wavelength parts of the gradient are removed. Accordingly, we could obtain long-wavelength velocity models from real marine data. An inversion example of the Gulf of Mexico data demonstrated this property of macro-velocity generation in the Laplace domain.

Inversion of real land data is a challenge to the Laplace-domain inversion. Land-data inversion results can show artificial high-wavenumber structures near the surface area. Further study of land data inversion need to examine the effect of the short-wavelength features at the surface.

Acknowledgements

This work was financially supported by Shin's Geophysics.

References

Aki, K., and Richards, P. G., 2002. Quantitative Seismology, 2nd ed.: University Science Books.

Bunks, C., F. Saleck, S. Zaleski, and G. Chavent, 1995. Multiscale seismic waveform inversion: Geophysics, **60**, 1457–1473.

Cohen, G., 2002. Higher-order numerical methods for transient wave equations: Springer.

Ha, W., Y. H. Cha, and C. Shin, 2010. A comparison between Laplace domain and frequency domain methods for inverting seismic waveforms: Exploration Geophysics, **41**, 189-197.

Jannane, M., W. Beydoun, E. Crase, D. Cao, and Z. Koren, 1989. Wavelengths of earth structures that can be resolved from seismic reflection data: Geophysics, **54**, 906-910.

Marfurt, K. J., 1984. Accuracy of finite-difference and finite-element modeling of the scalar and elastic wave equations: Geophysics, **49**, 533-549.

Officer, C. B., 1958. Introduction to the theory of sound transmission: McGraw-Hill.

Pyun, S., W. Son, and C. Shin, 2011. 3D acoustic waveform inversion in the Laplace domain using an iterative solver: Geophysical Prospecting, **59**, 386-399.

Schneider, W. A., 1978. Integral formulation for migration in two and three dimensions: Geophysics, **43**, 49-76.

Shin, C., and Y. Cha, 2008. Waveform inversion in the Laplace domain: Geophysical Journal International, **173**, 922-931.

Shin, C., and W. Ha, 2008. A comparison between the behavior of objective functions for waveform inversion in the frequency and Laplace domains: Geophysics, **73**, VE119-VE133.

Shin, C., and D. Min, 2006. Waveform inversion using a logarithmic wavefield: Geophysics, **71**, R31-R42.

Tarantola, A., 1984. Inversion of seismic-reflection data in the acoustic approximation: Geophysics, **49**, 1259–1266.

Virieux, J., and S. Operto, 2009. An overview of full-waveform inversion in exploration geophysics: Geophysics, **74**, WCC1-WCC26.